Earth and Planetary Science Letters 361 (2013) 249–257

Contents lists available at SciVerse ScienceDirect

Earth and Planetary Science Letters

journal homepage: www.elsevier.com/locate/epsl

Effects of Fe-enrichment on the equation of state and stability of $(Mg,Fe)SiO_3$ perovskite

Susannah M. Dorfman [a,*], Yue Meng [b], Vitali B. Prakapenka [c], Thomas S. Duffy [a]

[a] Department of Geosciences, Princeton University, Princeton, NJ 08544, USA
[b] High-Pressure Collaborative Access Team, Carnegie Institution of Washington, 9700 South Cass Avenue, Argonne, IL 60439, USA
[c] Center for Advanced Radiation Sources, The University of Chicago, 9700 South Cass Avenue, Argonne, IL 60439, USA

ARTICLE INFO

Article history:
Received 16 February 2012
Received in revised form
17 September 2012
Accepted 15 October 2012
Editor: L. Stixrude
Available online 8 December 2012

Keywords:
perovskite
post-perovskite
lower mantle
D″ region

ABSTRACT

Fe-rich natural orthopyroxenes with compositions of $(Mg_{0.61}Fe_{0.38}Ca_{0.01})SiO_3$ (Fe#38) and $(Mg_{0.25}Fe_{0.74}Ca_{0.01})SiO_3$ (Fe#74) were studied at pressures up to 155 GPa and temperatures up to 3000 K. Single-phase orthorhombic $GdFeO_3$-type perovskite was synthesized by heating to ~2000 K at 63 GPa for the Fe#38 composition and at 72 GPa for the Fe#74 composition. At lower pressures, heating both compositions resulted in a mixture of perovskite, SiO_2 and (Mg,Fe)O. These measurements provide new constraints on the dependence of $(Mg,Fe)SiO_3$ perovskite stability on pressure and composition. Upon further compression and heating at 89 and 99 GPa, Fe#38 and Fe#74 perovskites transformed to two-phase mixtures of perovskite and post-perovskite, consistent with previous findings that increasing Fe content lowers the transition pressure. The volume of $(Mg,Fe)SiO_3$ perovskites increases linearly with Fe-content. Volume data were fit to the Birch–Murnaghan equation of state. The bulk modulus at 80 GPa is 550–560 GPa for both Fe-rich perovskites, comparable to or slightly higher than the values measured for $MgSiO_3$ perovskite at this pressure, indicating that the bulk modulus of perovskite is not strongly sensitive to Fe content.

1. Introduction

Recent tomography studies of Earth's mantle have identified distinct dense regions near the core–mantle boundary with slow shear wave speed but high bulk sound speed (*e.g.* Trampert et al., 2004). The major chemical variable related to density variations in Earth's mantle is Fe-content. Fe-enrichment in the deep mantle could be generated by a variety of mechanisms including mixing of iron and iron alloys from the core with mantle silicate (Knittle and Jeanloz, 1989, 1991; Dubrovinsky et al., 2003) or sequestration of dense material during mantle crystallization (Labrosse et al., 2007; Lee et al., 2010) or convection (Williams and Garnero, 1996; McNamara and Zhong, 2005; Dobson and Brodholt, 2005). The chemistry of these heterogeneities and their role in geodynamics and Earth history cannot be determined from their observed properties without experimental measurements of the effects of Fe on phase equilibria and physical properties in the lower mantle.

Previous work has shown that the dominant phase of the lower mantle, $(Mg,Fe)SiO_3$ perovskite (Pv), can accommodate no more than ~12% $FeSiO_3$ at the pressures and temperatures of the top of the lower mantle (Fei et al., 1996). With increasing pressure and temperature, the Fe-content of the Pv increases to greater than 50% at 85 GPa (Fei et al., 1996; Mao et al., 1997; Tateno et al., 2007; Tange et al., 2009). Previous experiments on pure $FeSiO_3$ have observed a breakdown to FeO and SiO_2 at 20 GPa (Ming and Bassett, 1975) and at pressures as high as 149 GPa (Fujino et al., 2009). Thermodynamic models (Stixrude and Lithgow-Bertelloni, 2011) predict the solubility of $FeSiO_3$ in Pv increases with pressure up to 50–70% at 90–120 GPa. However, the pressure dependence of Fe-solubility in Pv above 50 GPa is not well-constrained.

The recently discovered $CaIrO_3$-type $(Mg,Fe)SiO_3$ post-perovskite (pPv) (*Cmcm*, Murakami et al., 2004; Oganov and Ono, 2004) is of great interest for its potential role in complex structures observed at the Earth's core-mantle boundary (Shim, 2008). The pPv phase is stable near the core-mantle boundary and can accommodate at least 80% $FeSiO_3$ (Mao et al., 2005). An alternate post-perovskite structure (*Pmcm*) has been proposed for an Fe-rich ($(Mg_{0.6}Fe_{0.4})SiO_3$) composition (Yamanaka et al., 2010).

$MgSiO_3$ has been observed to transform to the post-perovskite structure at 107–126 GPa, depending on the pressure scale used (Murakami et al., 2004; Hirose et al., 2006). The effect of Fe on the relative stability of the Pv and pPv phases is controversial. This is likely due to differences in pressure calibration (Tateno et al., 2007; Shim, 2008), chemical diffusion due to temperature gradients

* Corresponding author. Now at Earth and Planetary Science Laboratory, École Polytechnique Fédérale de Lausanne, CH-1015 Lausanne, Switzerland.
E-mail address: susannah.dorfman@epfl.ch (S.M. Dorfman).

0012-821X/$ - see front matter © 2012 Elsevier B.V. All rights reserved.
http://dx.doi.org/10.1016/j.epsl.2012.10.033

(Fialin et al., 2009; Sinmyo and Hirose, 2010) and the sluggish kinetics of the Pv–pPv transition (Shim et al., 2004; Mao et al., 2005; Shieh et al., 2006). In a $(Mg_{0.6}Fe_{0.4})SiO_3$ composition, a Pv–pPv mixture was observed at only 100 GPa (Mao et al., 2004). This may indicate a decrease in the transition pressure due to Fe-content and that the Pv and pPv phases coexist over a broad pressure range. However, other experiments show a weak increase in pPv transition pressure due to Fe (Hirose et al., 2006; Tateno et al., 2007). Theoretical predictions support the stability of Fe-rich pPv at lower pressures than Fe-poor pPv (Caracas and Cohen, 2005; Mao et al., 2005; Ono and Oganov, 2005; Stackhouse et al., 2006; Caracas and Cohen, 2008). The Pv–pPv phase boundaries depend strongly on the partitioning of Fe between these two phases (Stixrude and Lithgow-Bertelloni, 2011), which is also debated (Kobayashi et al., 2005; Auzende et al., 2008; Hirose et al., 2008; Andrault et al., 2010; Sinmyo et al., 2011). The resolution of this controversy will have implications for the interpretation of the observed sharp D″ seismic discontinuity (Lay et al., 1998; Wysession et al., 1998) and the detection of Fe-rich chemical heterogeneities in the lower mantle.

The effects of Fe on the equation of state of $(Mg,Fe)SiO_3$ perovskite have important implications for the interpretation of seismic wave speed variations in the mantle. Previous work on $(Mg,Fe)SiO_3$ Pv (Lundin et al., 2008) with 0%, 9% and 15% $FeSiO_3$ found no significant difference in compressibility. However, Mao et al. (2011) report that the isothermal bulk modulus of Pv with 25% $FeSiO_3$ is $\sim$20% larger at high pressures than that of the $MgSiO_3$ end-member. There have been no determinations of the bulk modulus of Pv with higher iron content.

Pressure-induced electronic spin transitions have been reported in X-ray emission spectroscopy and nuclear forward scattering measurements of $(Mg,Fe,Al)(Fe,Al,Si)O_3$ perovskites (Badro et al., 2004; Jackson et al., 2005; McCammon et al., 2010; Lin et al., 2008; Catalli et al., 2010; McCammon et al., 2008; Mao et al., 2011) and post-perovskites (Lin et al., 2008) and (Mg,Fe)O magnesiowüstite (Badro et al., 2003). However, there are almost no compression data on Fe-rich ($>$ 25 mol% Fe) silicates and thus any possible effects of a spin transition on compressibility and equation of state for such samples are unknown.

In this study, we evaluate the effects of Fe on phase boundaries and equations of state in the $(Mg,Fe)SiO_3$ system with 9–74% $FeSiO_3$. We use identical experimental protocols (pressure calibrant, quasi-hydrostatic media, heating conditions) for all compositions. We explore a wide compositional range for the maximum solubility of $FeSiO_3$ and its effect on the equation of state of $(Mg,Fe)SiO_3$ Pv. We also constrain the pressure interval of the Pv–pPv transition for these compositions to assess the effect of Fe on the phase boundary.

2. Method

Natural $(Mg,Fe)SiO_3$ orthopyroxene crystals (typical dimensions $100 \times 200 \times 400$ μm) isolated from charnockites (Madras, India) were obtained from the Princeton mineral collection. The geological environment, method of separation, and chemical composition were described by Subramaniam (1962). Orthopyroxenes with Fe/(Mg+Fe+Ca), or Fe#, 38 and 74 were selected for this study. We re-analyzed selected samples by electron microprobe (Table 1) and found good agreement with previous results. Microprobe analysis showed Fe#38 grains were banded with a few percent 1–10 μm quartz and Fe#74 grains contained a few percent of exsolved clinopyroxene (Ca#46, Fe#34, Mg#40) lamellae. An additional natural orthopyroxene (cm-scale single crystal, unknown origin) with Fe#9 (Table 1) was also used.

Crystals were ground to a few μm grain size and mixed with 1–5 μm Au powder as pressure calibrant (Fei et al., 2007).

Table 1
Microprobe results for orthopyroxene compositions used, including oxide weight percents and normalized molar percents of Mg, Fe and Ca. Orthopyroxenes isolated from charnockites (ch.) are labeled as in Subramaniam (1962). Compositional measurements varied between grains with a standard deviation $< 1\%$. Fe_2O_3 weight percent was calculated to balance charge.

Sample	Ch.29 opx	Ch.114 opx	Opx 1
MgO	7.91	21.07	35.17
FeO	41.64	23.63	6.13
Fe_2O_3	0.30	0.22	–
Al_2O_3	0.69	1.23	0.21
SiO_2	47.92	52.07	58.19
CaO	0.57	0.52	0.18
MnO	0.80	0.42	0.22
Total	99.92	99.40	100.10
Mg#	24.9	60.5	90.8
Fe#	73.8	38.4	8.9
Ca#	1.3	1.1	0.3

Samples were dried overnight in an oven at 100 °C. Compacts of the sample–Au mixture were loaded in diamond anvil cells with either NaCl or Ne as a pressure-transmitting and insulating medium. Samples prepared for Ne loading were supported by a NaCl tripod allowing gas to flow underneath. Ne was loaded at high pressure using the GSECARS/COMPRES gas loading system (Rivers et al., 2008). Diamonds with 200 μm or 75–100 μm culets were used to achieve pressures up to 80 GPa and up to 155 GPa, respectively. Re gaskets were preindented to 25–30 μm and sample chambers of approximately one half the culet diameter were cut using an electrical discharge machine or the GSECARS laser drilling system.

Double-sided laser heating experiments with *in situ* X-ray diffraction were performed at beamlines 13-ID-D and 16-ID-B of the GSECARS and HPCAT sectors of the Advanced Photon Source. Temperatures were measured on both sides by spectroradiometry (Shen et al., 2001). Laser power was adjusted independently on upstream and downstream sides to reduce measured temperature differences to $\sim$100 K. Heating durations were typically 30–60 min. Over this time, temperatures typically varied by $\sim$100–300 K. Diffraction patterns were collected on a MarCCD. The 2D images were processed with Fit2D software (Hammersley et al., 1996). Diffraction peaks were fit to Voigt lineshapes. Lattice parameters were obtained by least-squares fit of peak positions. Rietveld refinement of selected patterns was conducted using GSAS and EXPGUI software (Larson and Von Dreele, 2000; Toby, 2001).

3. Results

3.1. Fe solubility in $(Mg,Fe)SiO_3$ perovskite

Samples of all three compositions were compressed to 44–80 GPa and subsequently heated. During 30 min of laser heating to 2100–2200 K at 64 and 80 GPa, $(Mg,Fe)SiO_3$ compositions with 38% and 74% $FeSiO_3$, respectively, were transformed to a single-phase, orthorhombic $GdFeO_3$-type (*Pbnm*) perovskite. All diffraction peaks were indexed to orthorhombic $GdFeO_3$-type perovskite, NaCl, Ne or Au (Fig. 1). Observed perovskite lattice spacings from representative diffraction patterns are given in supplementary table 1. For Fe#74 perovskite, the $GdFeO_3$ structure was confirmed by full-profile refinement (Fig. 2). Lattice parameters and peak profiles were refined for all phases. Texture was refined for NaCl B2 and Au phases by the spherical harmonic method (order 2 or 4) and was within error of random. Atomic

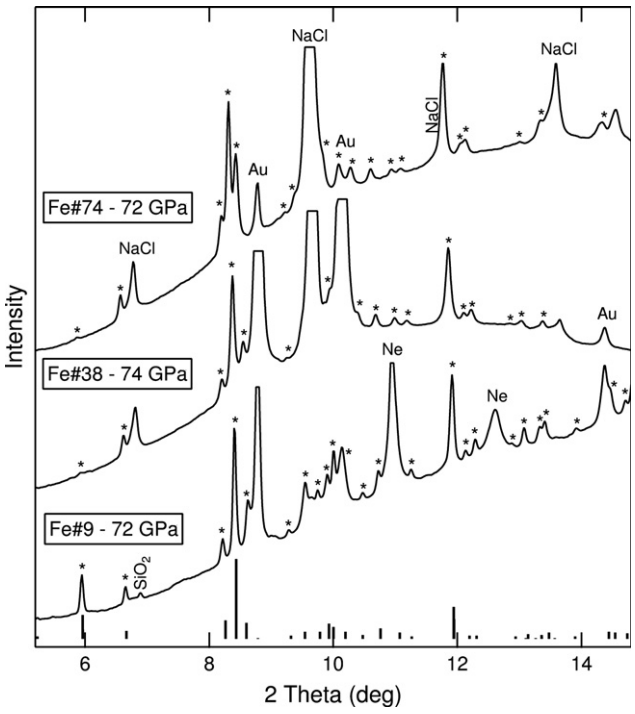

Fig. 1. Diffraction patterns from (Mg,Fe)SiO_3 compositions at 74–77 GPa and 300 K after laser heating quench. All peaks are indexed to orthorhombic $GdFeO_3$-type perovskite (peak locations and relative intensities are indicated at bottom of figure), Au, NaCl or Ne. Note that the (020), (112), (200) triplet near $2\theta = 8.5^\circ$ and the (023), (221) doublet just above $2\theta = 12^\circ$ become more closely spaced with increasing Fe-content. Intensity differences between compositions (*e.g.* the (110)/(002) doublet near 6°) are due to Fe-content and preferred orientation. More diffraction peaks are resolved near 10° for Fe#9 composition due to lower intensity of NaCl B2 (110) and Au (200) lines. $\lambda = 0.3344$ Å for these experiments.

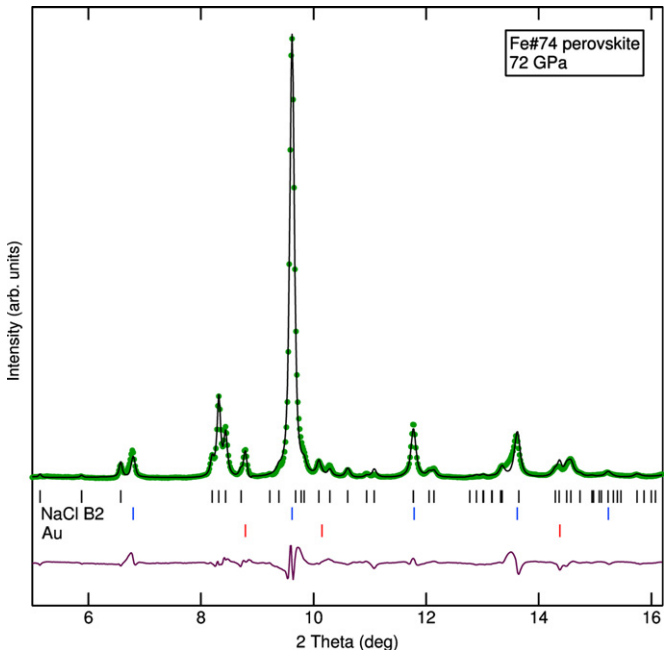

Fig. 2. Full-profile refinement of Fe#74 perovskite at 72 GPa. Intensity data (green dots) are fit (black line) with residual (purple line) to orthorhombic $GdFeO_3$-type perovskite (black sticks), NaCl B2 phase (blue sticks) and Au (red sticks). Lattice parameters for the perovskite phase are $a = 4.5461$ Å, $b = 4.6775$ Å, $c = 6.5239$ Å and $V = 138.727$ Å^3. $\lambda = 0.3344$ Å for this experiment. (For interpretation of the references to color in this figure caption, the reader is referred to the web version of this article.)

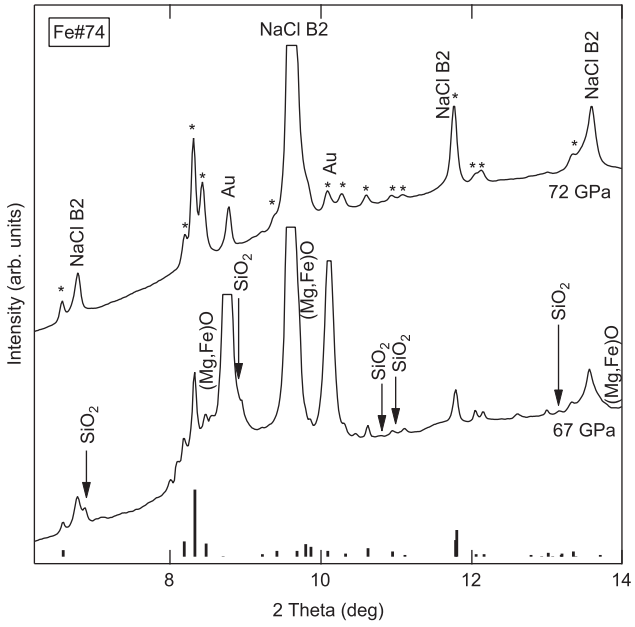

Fig. 3. Selected diffraction patterns for Fe#74 perovskite showing transition from perovskite to perovskite plus oxide mixture on decompression. Orthorhombic $GdFeO_3$-type perovskite peaks are marked with asterisks and reference pattern is below. At 72 GPa, all peaks can be indexed to perovskite, NaCl medium or Au calibrant, but after heating at 67 GPa, $CaCl_2$-type SiO_2 and (Mg,Fe)O peaks are also observed. $\lambda = 0.3344$ Å for these experiments.

positions refined for the perovskite phase are given in supplementary table 2 and are similar to values previously obtained for $MgSiO_3$ perovskite (Ross and Hazen, 1990). Refined lattice parameters are in good agreement with values derived from peak fitting.

The Fe#74 sample was compressed directly to 80 GPa without heating. Perovskite peaks grew during heating at 1860–2140 K and were retained upon quench. The sample was then decompressed with heating to ~ 2000 K for 30 min at ~ 3 GPa intervals. At 68–71 GPa and 2020 ± 50 K after 30 min of heating, single-phase perovskite was still observed. After the next decompression step, SiO_2 and (Mg,Fe)O diffraction peaks appeared during heating at 2010 ± 100 K and 64–67 GPa. Upon temperature quench, perovskite, SiO_2 and (Mg,Fe)O were observed (Fig. 3).

When the Fe#38 sample was compressed to 44 GPa and heated to 1980 ± 70 K, it transformed to a mixture of perovskite, stishovite SiO_2 and magnesiowüstite (Mg,Fe)O. With increasing pressure and subsequent heating to 1800–2200 K, the stishovite/$CaCl_2$-type SiO_2 and (Mg,Fe)O diffraction peaks decreased in intensity, indicating gradual dissolution of the oxides into the perovskite phase with increasing pressure until full solid solution is reached. Oxide peaks were observed at 1940 ± 70 K and 58 GPa, but disappeared at 1930 ± 150 K and 64 GPa. The quenched sample at 64 GPa showed only perovskite.

Although the Fe#74 sample contains lamellae of Ca-rich clinopyroxene, no $CaSiO_3$ perovskite peaks were observed. The Ca component was thus dissolved in the Fe-rich perovskite or below the detection limit. X-ray diffraction may not be able to detect $< 5\%$ $CaSiO_3$ perovskite. These observations are consistent with $< 5\%$ clinopyroxene in the mixed sample powder.

These observations and previous work are summarized in a phase diagram for the (Mg,Fe)SiO_3 system (Fig. 4). For the Fe#38 composition, 64 GPa should be considered an upper bound to the

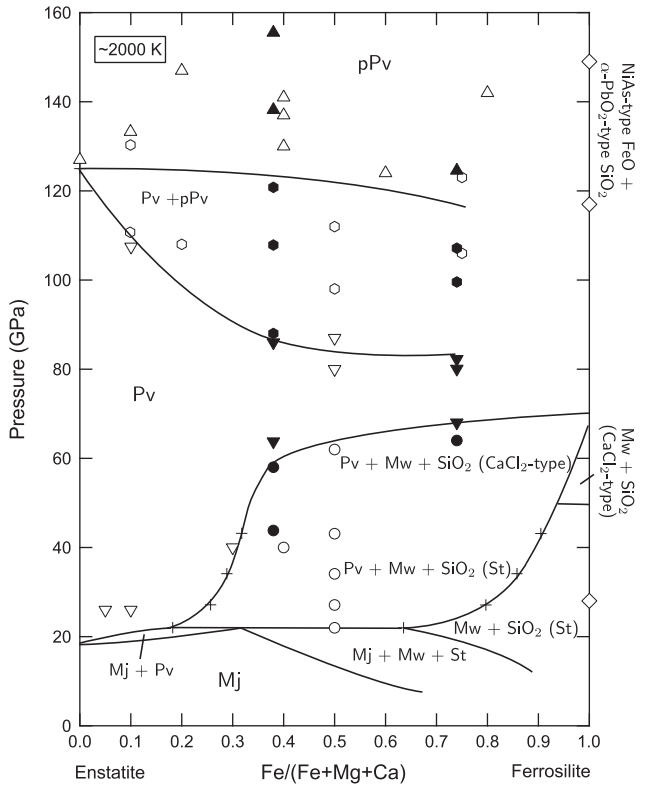

Fig. 4. Schematic phase diagram for $(Mg,Fe)SiO_3$ system. Phases include majorite (Mj), magnesiowüstite (Mw), stishovite (St), perovskite (Pv) and post-perovskite (pPv). Pressures at which various phase assemblages were found in this study (filled symbols) and previous work (Liu, 1976; Mao et al., 2004–2006; Tateno et al., 2007; Catalli et al., 2009; Fujino et al., 2009; Tange et al., 2009; Yamanaka et al., 2010) (open symbols) are plotted as follows: post-perovskite, up-triangles; perovskite plus post-perovskite, hexagons; perovskite, down-triangles; perovskite plus oxides, circles; oxides, diamonds. Crosses indicate compositions of two phases formed from $(Mg_{0.5}Fe_{0.5})SiO_3$ composition.

perovksite-plus-oxide to perovskite phase boundary due to the slow kinetics of diffusion in reactions between multiple phases. For similar reasons, in the Fe#74 composition 67 GPa is a lower bound for the phase boundary. For a synthetic Fe#50 sample, intermediate in Fe-content relative to the compositions studied in this work, Tateno et al. (2007) observed single-phase perovskite at 85 GPa and 1800–2000 K. However, a mixture of perovskite and oxides was obtained at 79 GPa and 2350 K, a higher pressure than our constraint for the more Fe-rich Fe#74 sample. Differences in pressure calibration between this work and Tateno et al. (2007) should be no more than 3 GPa due to consistency between Au scales by Tsuchiya (2003) and Fei et al. (2007). The discrepancy between these studies may be due to heating conditions/temperature gradients.

Combined with previous observations of much lower solubility of $FeSiO_3$ in $(Mg,Fe)SiO_3$ perovskite up to 40–50 GPa (Fei et al., 1996; Mao et al., 1997; Tange et al., 2009), our results suggest a sharp increase in the solubility of the $FeSiO_3$ component at 50–70 GPa (Fig. 4), where $(Mg,Fe)SiO_3$ Pv can accommodate at least 74% $FeSiO_3$. This high solubility of $FeSiO_3$ is consistent with previous observations of at least 50% $FeSiO_3$ in Pv (Tateno et al., 2007) and 80% in pPv (Mao et al., 2005). The only constraints at higher Fe content come from studies of $FeSiO_3$. At pressures below 50 GPa, $FeSiO_3$ disproportionates into FeO and SiO_2 (Ming and Bassett, 1975; Fujino et al., 2009). Experiments have also reported disproportionation at pressures above 115 GPa (Fujino et al., 2009). At deep lower mantle pressures, the solubility limit of $FeSiO_3$ in $(Mg,Fe)SiO_3$ Pv remains unknown.

3.2. Perovskite–post-perovskite transition

Upon compression to higher pressures, perovskite remained stable as a single-phase during and after heating to 2150 ± 100 K for 30 minutes at 87 GPa and 80–82 GPa in Fe#38 and #74 compositions, respectively. The post-perovskite (pPv) (022) line was observed in these compositions after heating to 2000–2600 K for 30–60 minutes at 89 GPa and 99 GPa (Fig. 5, supplementary figure 1). These pressures are consistent with observations of pPv at 100 GPa in the Fe#40 composition by Mao et al. (2005). However, Tateno et al. (2007) reported the Fe#50 composition remains single-phase Pv at 85–108 GPa with no pPv peaks below 106 GPa and 1410 K. Pressure scales used in these studies (Jamieson et al., 1982; Tsuchiya, 2003; Fei et al., 2007) have been found to be consistent within 3 GPa (Shim, 2008; Dorfman et al., 2012). The transition from perovskite to post-perovskite is known to be sluggish (Shim, 2008) and this could potentially lead to an overestimate of the transition pressure if perovskite is retained metastably in the pPv field.

Single-phase post-perovskite was observed in Fe#38 and Fe#74 compositions at 130–156 GPa. Fe#38 post-perovskite was synthesized at 155 GPa during 60 minutes of heating to 1800–2100 K and remained on decompression to 138 GPa with heating to 1700–2050 K for 15 min (supplementary figure 1, supplementary table 3). The nature of the pPv phase in Fe-rich compositions has been controversial with a recent report in a Fe#40 composition of a new *Pmcm* pPv structure (Yamanaka et al., 2010). Yamanaka et al. (2010) observed differences in diffraction intensities due to ordering in the

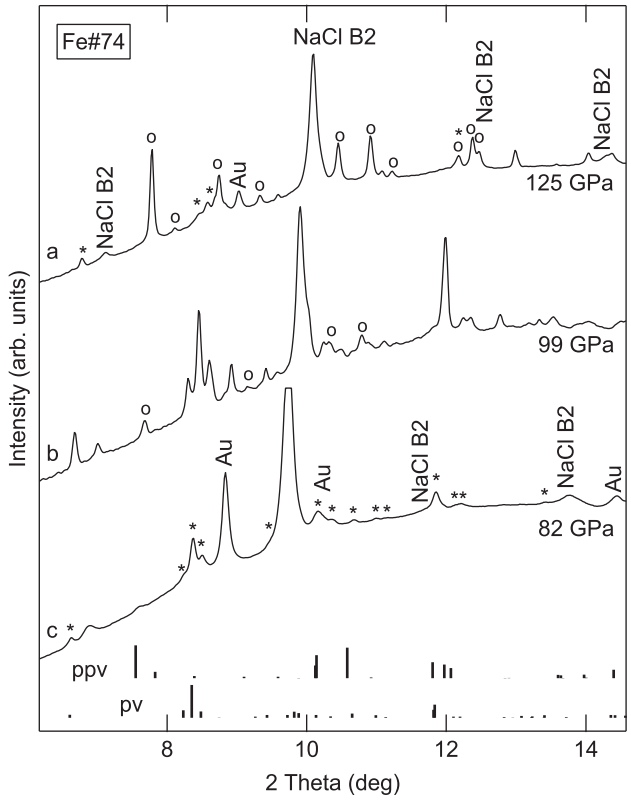

Fig. 5. Selected diffraction patterns for Fe#74 perovskite illustrating transition from perovskite to post-perovskite on compression. Orthorhombic $GdFeO_3$-type perovskite peaks are marked with asterisks, orthorhombic $CaIrO_3$-type post-perovskite peaks are marked with circles and reference patterns are below. All peaks can be indexed to perovskite, post-perovskite, NaCl medium and Au calibrant. At 82 GPa, perovskite is observed. At 99 GPa, perovskite is still dominant but also apparent are the strongest post-perovskite peaks, (022) and (131). At 125 GPa, the dominant phase is post-perovskite. $\lambda = 0.3344$ Å for these experiments.

Mg/Fe site and suggested additional peaks forbidden in *Cmcm* symmetry could also appear in Fe-rich compositions, including (120), (013) and (033). We were not able to determine whether the subtle differences in intensity observed by Yamanaka et al. (2010) were also exhibited by our samples. We do observe several additional weak peaks that could be consistent with the (120), (013) and (033) peaks of the *Pmcm* phase (supplementary figure 1). An additional stronger peak was observed with $d=1.77$–1.78 Å, which would have been overlapped by the Pt calibrant in Yamanaka et al. (2010) and is not consistent with either the *Pmcm* or *Cmcm* post-perovskite structures. These peaks are also inconsistent with α-PbO_2-type SiO_2, (Mg,Fe)O and Fe metal. However, least-squares refinement of pPv lattice parameters including the three new peaks yielded a poorer fit with standard deviations of the lattice parameters a factor of 10 higher. We thus cannot confirm the observation of a *Pmcm* phase or the origin of the weak, unexplained peaks in our pattern.

On decompression of Fe#38 post-perovskite to 121 GPa, the perovskite (111) peak appeared after 10 min heating at 1800–2100 K (supplementary figure 1). This pressure is a lower bound to the stability of single-phase pPv. In the Fe#74 composition, pPv peaks were observed to grow with increasing pressure and successive heating from 82 to 125 GPa (Fig. 5). At 82 GPa, Pv peaks were accompanied by a few weak diamond spots at $\sim 7.5-7.6^{\circ}$. These reflections are near the expected position for the pPv phase (022) plane but were also present before any heating and so are not related to pPv. At 99 GPa after heating to 2320 K for 25 minutes, the pPv (022) line is clear and additional pPv lines are observed (Fig. 5). Heating to 1950–2350 K for 40 min at 125 GPa produced dominant pPv (Fig. 5), but weak Pv peaks persisted. The strong growth of the pPv phase at 125 GPa suggests pPv is stable at this pressure in the Fe#74 composition. These observations may indicate that Pv coexists with pPv over 30–40 GPa (corresponding to 600–800 km depth in the Earth) in the Fe#38 and 74 compositions (Fig. 4), consistent with a broad two-phase perovskite–post-perovskite region in Fe-rich compositions.

Perovskite–post-perovskite coexistence over a wide range of pressures implies strong partitioning of Fe between the perovskite and post-perovskite phases. However, observed *d*-spacings for Pv and pPv at 80–108 GPa are consistent with Fe-enrichment in both phases. Lattice parameters for the Pv phase (discussed in more detail below and shown in Fig. 6) show no apparent increase in compressibility due to loss of Fe in this pressure range. For Fe#38 pPv, the *d*-spacing of the (022) plane in the two-phase region is consistent with recent measurements of Fe#40 pPv by Zhang et al. (2012), supporting no strong partitioning of Fe into or out of the pPv phase. Recent studies have produced conflicting results for the partitioning of Fe between Pv and pPv phases: while some TEM studies of recovered samples find that Fe prefers pPv to Pv (Kobayashi et al., 2005; Auzende et al., 2008), others suggest the opposite (Hirose et al., 2008; Andrault et al., 2010; Sinmyo et al., 2011). The observation of Fe-rich pPv at pressures below 1 Mbar indicates the need for direct study of partitioning between perovskite and post-perovskite at these conditions.

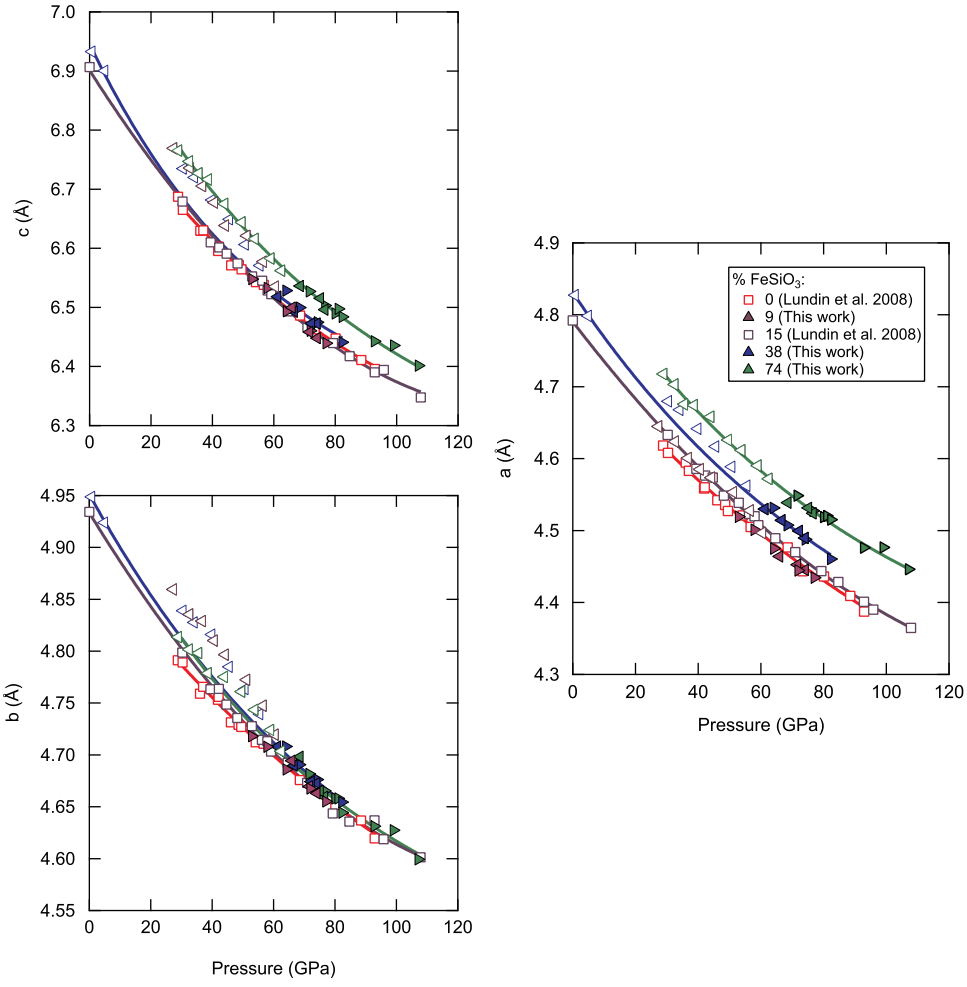

Fig. 6. Lattice parameters *a*, *b* and *c* for perovskites measured upon compression (right-pointing triangles) and decompression (left-pointing triangles) compared with previous work (Lundin et al., 2008). Open triangles: data not used in equation of state fit due to deviatoric stress.

3.3. Equation of state

Perovskites were synthesized from Fe#9, 38 and 74 compositions at 53, 64–74 and 77–82 GPa. Diffraction data were collected at pressures ranging from 0.7 to 107 GPa upon compression and decompression in $\sim 1-7$ GPa steps. In order to minimize differential stress, we loaded our samples in a quasi-hydrostatic medium (either NaCl or Ne). For samples loaded in NaCl medium, we performed laser annealing after each compression or decompression step. Differential stress indicated by peak widths and lattice strain in Au after annealing was comparable to measurements by Takemura and Dewaele (2008) in a He medium. Samples loaded in Ne medium were annealed only above 70 GPa to prevent breakdown of the Fe-rich perovskite at lower pressures. The Fe#38 sample loaded in Ne remained in the perovskite structure upon decompression to 0.7 GPa but the sample was lost on further unloading. The Fe#74 similarly was quenched to 29 GPa but lost below this point. Trace stishovite/$CaCl_2$-type SiO_2 (110) peaks were observed in some diffraction patterns in all compositions. Weak post-perovskite (022) peaks were observed above 82 GPa for the Fe#74 composition. Perovskite unit cell volume data are shown in Fig. 7.

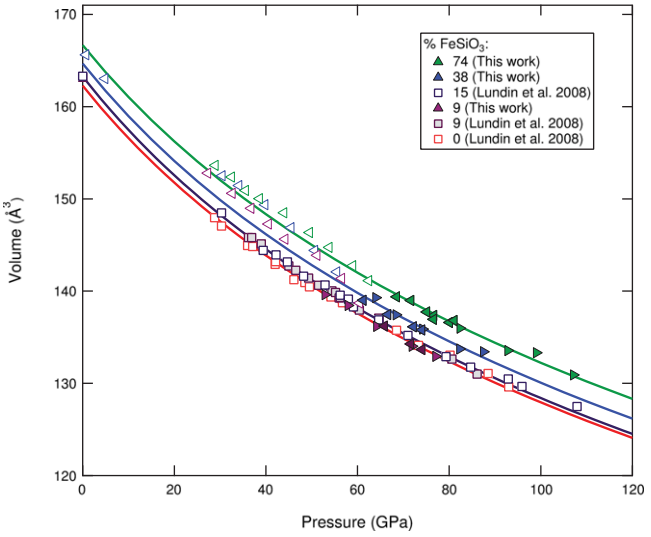

Fig. 7. Unit cell volumes measured on compression (right-pointing triangles) and decompression (left-pointing triangles) for $(Mg,Fe)SiO_3$ perovskites and Birch–Murnaghan equation of state fits. Open triangles were not used for equation of state fits due to significant deviatoric stresses. Volumes indicated by open squares are from Lundin et al. (2008). Pressures for this and previous work were determined by Au scale of Fei et al. (2007).

Unit cell volumes for Fe#9 perovskite measured in this study are in good agreement with Lundin et al. (2008). The expansion of the $(Mg,Fe)SiO_3$ perovskite unit cell is approximately linear with Fe-content in the range of pressures studied here. The datum reported for Fe#40 perovskite by Zhang et al. (2012) at 83 GPa coincides with our data for Fe#38 perovskite.

Unit cell volumes for Fe#9, 38 and 74 perovskites over ranges of 53–77, 61–88 and 69–107 GPa respectively were fit to the third-order Birch–Murnaghan equation of state (Fig. 7) and the results are given in Table 2. Volume data measured below ~ 60 GPa (*i.e.* outside the Pv stability field) were not used in equation of state fits due to evidence for differential stress. Equation of state fits for the Fe#74 composition were not significantly different with and without volume data measured above 82 GPa (with trace pPv). Fitting the high-pressure data with the zero-pressure parameters of the Birch–Murnaghan equation of state, volume, V_0, isothermal bulk modulus, K_0, and the pressure derivative of the bulk modulus, K_0', entails a long extrapolation. This increases uncertainty in the equation of state fit due to parameter trade-offs (*e.g.* Angel, 2000). V_0 for $(Mg,Fe)SiO_3$ perovskite has been constrained for compositions with Fe# 0–32 by previous studies (Yagi et al., 1979; Ito and Yamada, 1982; Mao et al., 1991; Fei et al., 1996; Lundin et al., 2008; Tange et al., 2009). We fit these values to a linear relationship giving: $V_0 = 162.5\ \text{Å}^3 + (0.0569\ \text{Å}^3) \times (\text{Fe\#})$, and used this equation to obtain V_0 for all compositions. Equation of state fits were performed with V_0 and K_0' fixed (Table 2).

The bulk modulus was also determined at high pressure by taking a volume derivative of the Birch–Murnaghan equation (Jackson, 1998). For all our compositions, values for the bulk modulus at 80 GPa, K_{80}, ranged from 540 to 564 GPa. Stiffening of perovskite due to Fe-content is comparable to the error for this measurement. These findings are consistent with other studies that find no significant effect of Fe on compressibility of Pv (Mao et al., 1991; Lundin et al., 2008), but inconsistent with recent work by Mao et al. (2011) for the Fe#25 composition. A spin transition in Fe^{3+} was suggested as the cause of the bulk modulus increase by Mao et al. (2011), although the presence of differential stress may also result in an anomalously large bulk modulus. For a broad range of iron content, we find that Fe-enrichment does not significantly affect the bulk compressibility of the Pv phase in the deep lower mantle.

The pressure dependence of the lattice parameters for $(Mg,Fe)SiO_3$ perovskites is shown in Fig. 6. Our results for the Fe#9

Table 2
Birch–Murnaghan equation of state parameters for $(Mg,Fe)SiO_3$ perovskite. $*$=parameter fixed in fit. Subscript on V and K indicates pressure in GPa, *i.e.* V_{80} is the unit cell volume at 80 GPa. V_{80} and K_{80} were computed from zero-pressure equation of state parameters using the Birch–Murnaghan equation and its volume derivative (Jackson, 1998). Errors for this work are determined by varying K_0' from 3.5 to 4.5. Ranges given for Lundin et al. (2008) are from Au calibration by Dewaele et al. (2004) vs. Tsuchiya (2003).

Reference	Fe#	V_0 (Å^3)	K_0 (GPa)	K_0'	V_{80} (Å^3)	K_{80} (GPa)
This work	74	166.7*	271 ± 16	4*	136.73 ± 0.06	560 ± 20
This work	38	164.7*	264 ± 14	4*	134.47 ± 0.08	555 ± 25
This work	9	163.0*	251 ± 13	4*	132.20 ± 0.13	540 ± 25
Mao et al. (1991)	10	162.8	261	4	132.8	553
Fiquet et al. (2000)	0	162.3*	259.5	3.69	131.6	527
Andrault et al. (2001)	5	162.7	255.4	4*	132.3	547
Andrault et al. (2001)	0	162.4	248.8	4*	131.5	540
Lundin et al. (2008)	15	163.30	257–259 (1)	4*	132.9–133.1	549–557
Lundin et al. (2008)	9	163.18	257–259 (1)	4*	132.7–132.9	533–541
Lundin et al. (2008)	0	162.30	255–261 (1)	4*	132.4–132.6	545–578
Mao et al. (2011)	25	159.3(6)	335 (8)	4*	134.4	630
Mao et al. (2011)	0	162.4	260 (3)	3.5*	131.2	510

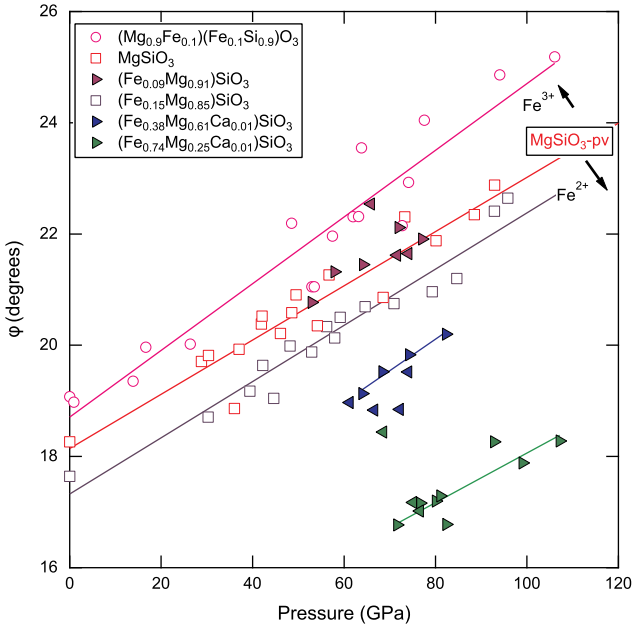

Fig. 8. Octahedral tilting angle (O'Keeffe et al., 1979), ϕ, for Fe-rich silicate perovskites. Data for $(Mg_{0.9}Fe_{0.1})(Fe_{0.1}Si_{0.9})O_3$ (Fe^{3+}-bearing) perovskite from Catalli et al. (2010) and for $MgSiO_3$ and $(Mg_{0.85}Fe_{0.15})SiO_3$ (Fe^{2+}-bearing) perovskite from Lundin et al. (2008).

composition are broadly comparable with earlier data for Fe#0–15 compositions (Lundin et al., 2008). The expansion of the unit cell volume of perovskite due to Fe incorporation is mainly reflected in the *a* and *c* lattice parameters. Fe has the strongest effect on the *a* lattice parameter of perovskite, as *a* increases by 1% and 2% relative to Fe#9 perovskite for the Fe#38 and Fe#74 compositions. The *c* lattice parameter appears to exhibit a non-linear dependence on Fe content. We observe that the *b* lattice parameter for perovskite is insensitive to Fe content for Fe#9, Fe#38, and Fe#74 samples. However, when samples were compressed or decompressed without laser annealing, *b* lattice parameter values became anomalously large relative to samples that were laser annealed (Fig. 6). These anomalous measurements coincide with diffraction peak broadening of 25–75% relative to annealed data. This enables us to identify the *b* parameter of perovskite as an indicator of the presence of differential stress, and such data were excluded from equation of state fits.

The ABO_3 perovskite structure is composed of corner-linked octahedra with A cations occupying the interstices. For smaller cations such as Mg and Fe, the framework collapses resulting in tilting of SiO_6 octahedra. Assuming rigid octahedra, the deformation of the perovskite lattice cell due to compression or cation substitution can be characterized by the octahedral tilting angle, ϕ (O'Keeffe et al., 1979). For the cubic perovskite structure, $\phi = 0$. We compute ϕ from the orthorhombic lattice parameters (O'Keeffe et al., 1979):

$$\phi = \cos^{-1}\left(\frac{\sqrt{2}a^2}{bc}\right) \quad (1)$$

For all $(Mg,Fe)SiO_3$ perovskites, tilting of the SiO_6 octahedra increases with pressure by $\sim 0.05^\circ$/GPa (Fig. 8). In previous work on $(Mg,Fe)(Fe,Si)O_3$ perovskite, the addition of Fe^{2+} was observed to reduce ϕ (Lundin et al., 2008) and Fe^{3+} to increase ϕ (Catalli et al., 2010). In our experiments, the observed decrease in ϕ with Fe-content is consistent with increasing Fe^{2+} in $(Mg,Fe)SiO_3$ perovskite (Fig. 8).

4. Summary

Single-phase orthorhombic $(Mg,Fe)SiO_3$ perovskite is stable for compositions with 9–74% $FeSiO_3$ at 72–89 GPa. Together with data from previous studies from 22 to 50 GPa, these results suggest a strong increase in the solubility of $FeSiO_3$ with pressure. Fe-rich perovskites with 38% and 74% $FeSiO_3$ were observed to transform to a mixture of perovskite and post-perovskite at pressures as low as 89 GPa. Above 130 GPa, single-phase post-perovskites were synthesized from Fe#38 and Fe#74 compositions. On compression and decompression, perovskite and post-perovskite were observed to coexist over a pressure range wider than 30 GPa.

Unit cell volumes of $(Mg,Fe)SiO_3$ perovskite were fit to the Birch–Murnaghan equation of state. The addition of Fe to the $(Mg,Fe)SiO_3$ perovskite structure has no measurable effect on bulk modulus. The measured equations of state of perovskites with Fe#38 and Fe#74 exhibit a smooth variation within the resolution of the data. Any electronic spin transition occurring in these compositions is either gradual or has too weak an effect on volume to be observed.

Acknowledgments

This work was supported by the NSF and the Carnegie-DOE Alliance Center. C.M. Holl assisted with beamline measurements. J. Delaney assisted with chemical analyses at the Rutgers University microprobe facility. S. Tkachev provided support for high-pressure gas loading. High-pressure gas loading was supported by COMPRES and GeoSoilEnviroCARS. P. Dera, K. Zhuravlev and I. Kantor assisted with beamline operations. Experiments were performed at GeoSoilEnviroCARS (Sector 13) and High Pressure Collaborative Access Team (HPCAT, Sector 16) at the APS. GeoSoil EnviroCARS is supported by the NSF – Earth Sciences (EAR-1128799) and DOE – Geosciences (DE-FG02-94ER14466). HPCAT is supported by CIW, CDAC, UNLV and LLNL through funding from DOE-NNSA and DOE-BES, with partial instrumentation funding by NSF. Use of the APS was supported by the U.S. Department of Energy, Office of Basic Energy Sciences, under Contract No. DE-AC02-06CH11357.

Appendix A. Supplementary materials

Supplementary data associated with this article can be found in the online version at http://dx.doi.org/10.1016/j.epsl.2012.10.033.

References

Andrault, D., Bolfan-Casanova, N., Guignot, N., 2001. Equation of state of lower mantle (Al,Fe)-$MgSiO_3$ perovskite. Earth Planet. Sci. Lett. 193, 501–508.
Andrault, D., Muñoz, M., Bolfan-Casanova, N., Guignot, N., Perrillat, J., Aquilanti, G., Pascarelli, S., 2010. Experimental evidence for perovskite and post-perovskite coexistence throughout the whole D″ region. Earth Planet. Sci. Lett., 90–96.
Angel, R.J., 2000. Equations of state. In: Hazen, R.M., Downs, R.T. (Eds.), High-Pressure, High-Temperature Crystal Chemistry. Reviews in Mineralogy and Geochemistry, vol. 41. Mineralogical Society of America, pp. 35–60.
Auzende, A., Badro, J., Ryerson, F.J., Weber, P.K., Fallon, S.J., Addad, A., Siebert, J., Fiquet, G., 2008. Element partitioning between magnesium silicate perovskite and ferropericlase: new insights into bulk lower mantle geochemistry. Earth Planet. Sci. Lett. 269, 164–174.
Badro, J., Fiquet, G., Guyot, F., Rueff, J., Struzhkin, V.V., Vankó, G., Monaco, G., 2003. Iron partitioning in Earth's mantle: toward a deep lower mantle discontinuity. Science 300 (5620), 789–791.
Badro, J., Rueff, J., Vanko, G., Monaco, G., Fiquet, G., Guyot, F., 2004. Electronic transitions in perovskite: possible nonconvecting layers in the lower mantle. Science 305 (5682), 383–386.

Caracas, R., Cohen, R.E., 2005. Effect of chemistry on the stability and elasticity of the perovskite and post-perovskite phases in the $MgSiO_3$–$FeSiO_3$–Al_2O_3 system and implications for the lowermost mantle. Geophys. Res. Lett. 32, L16310.

Caracas, R., Cohen, R.E., 2008. Ferrous iron in post-perovskite from first-principles calculations. Phys. Earth Planet. Inter. 168 (3–4), 147–152.

Catalli, K., Shim, S.-H., Prakapenka, V., 2009. Thickness and Clapeyron slope of the post-perovskite boundary. Nature 462 (7274), 782–785.

Catalli, K., Shim, S.-H., Prakapenka, V.B., Zhao, J., Sturhahn, W., Chow, P., Xiao, Y., Liu, H., Cynn, H., Evans, W.J., 2010. Spin state of ferric iron in $MgSiO_3$ perovskite and its effect on elastic properties. Earth Planet. Sci. Lett. 289 (1–2), 68–75.

Dewaele, A., Loubeyre, P., Mezouar, M., 2004. Equations of state of six metals above 94 GPa. Phys. Rev. B (Condens. Matter Mater. Phys.) 70 (9), 094112.

Dobson, D.P., Brodholt, J.P., 2005. Subducted banded iron formations as a source of ultralow-velocity zones at the core-mantle boundary. Nature 434 (7031), 371–374.

Dorfman, S.M., Prakapenka, V.B., Meng, Y., Duffy, T.S., 2012. Intercomparison of pressure standards (Au, Pt, Mo, MgO, NaCl and Ne) to 2.5 Mbar. J. Geophys. Res. 117 (B8), B08210.

Dubrovinsky, L., Dubrovinskaia, N., Langenhorst, F., Dobson, D., Rubie, D., Geszmann, C., Abrikosov, I.A., Johansson, B., Baykov, V.I., Vitos, L., Bihan, T.L., Crichton, W.A., Dmitriev, V., Weber, H., 2003. Iron–silica interaction at extreme conditions and the electrically conducting layer at the base of Earth's mantle. Nature 422 (6927), 58–61.

Fei, Y., Ricolleau, A., Frank, M., Mibe, K., Shen, G., Prakapenka, V.B., 2007. Toward an internally consistent pressure scale. Proc. Natl. Acad. Sci. 104 (22), 9182–9186.

Fei, Y., Wang, Y., Finger, L.W., 1996. Maximum solubility of FeO in $(Mg,Fe)SiO_3$-perovskite as a function of temperature at 26 GPa: implication for FeO content in the lower mantle. J. Geophys. Res. 101 (B5), 11525–11530.

Fialin, M., Catillon, G., Andrault, D., 2009. Disproportionation of Fe^{2+} in Al-free silicate perovskite in the laser heated diamond anvil cell as recorded by electron probe microanalysis of oxygen. Phys. Chem. Miner. 36 (4), 183–191.

Fiquet, G., Dewaele, A., Andrault, D., Kunz, M., Bihan, T.L., 2000. Thermoelastic properties and crystal structure of $MgSiO_3$ perovskite at lower mantle pressure and temperature conditions. Geophys. Res. Lett. 27 (1), 21–24.

Fujino, K., Nishio-Hamane, D., Suzuki, K., Izumi, H., Seto, Y., Nagai, T., 2009. Stability of the perovskite structure and possibility of the transition to the post-perovskite structure in $CaSiO_3$, $FeSiO_3$, $MnSiO_3$ and $CoSiO_3$. Phys. Earth Planet. Inter. 177 (3–4), 147–151.

Hammersley, A.P., Svensson, S.O., Hanfland, M., Fitch, A.N., Hausermann, D., 1996. Two-dimensional detector software: from real detector to idealised image or two-theta scan. High Pressure Res. 14, 235–248.

Hirose, K., Sinmyo, R., Sata, N., Ohishi, Y., 2006. Determination of post-perovskite phase transition boundary in $MgSiO_3$ using Au and MgO pressure standards. Geophys. Res. Lett. 33, L01310.

Hirose, K., Takafuji, N., Fujino, K., Shieh, S.R., Duffy, T.S., 2008. Iron partitioning between perovskite and post-perovskite: a transmission electron microscope study. Am. Miner. 93 (10), 1678–1681.

Ito, E., Yamada, H., 1982. Stability relations of silicate spinels, ilmenites, and perovskites. In: Akimoto, S., Manghnani, M.H. (Eds.), High-Pressure Research in Geophysics. Center for Academic Publications Japan, pp. 405–419.

Jackson, I., 1998. Elasticity, composition and temperature of the Earth's lower mantle: a reappraisal. Geophys. J. Int. 134 (1), 291–311.

Jackson, J.M., Sturhahn, W., Shen, G., Zhao, J., Hu, M.Y., Errandonea, D., Bass, J.D., Fei, Y., 2005. A synchrotron Mössbauer spectroscopy study of $(Mg,Fe)SiO_3$ perovskite up to 120 GPa. Am. Mineral. 90, 199–205.

Jamieson, J.C., Fritz, J.N., Manghnani, M.H., 1982. Pressure measurement at high temperature in X-ray diffraction studies: gold as a primary standard. In: Akimoto, S., Manghnani, M.H. (Eds.), High-Pressure Research in Geophysics. Center for Academic Publishing, pp. 27–48.

Knittle, E., Jeanloz, R., 1989. Simulating the core–mantle boundary: an experimental study of high-pressure reactions between silicates and liquid iron. Geophys. Res. Lett. 16 (7), 609–612.

Knittle, E., Jeanloz, R., 1991. Earth's core–mantle boundary: results of experiments at high pressures and temperatures. Science 251 (5000), 1438–1443.

Kobayashi, Y., Kondo, T., Ohtani, E., Hirao, N., Miyajima, N., Yagi, T., Nagase, T., Kikegawa, T., 2005. Fe-Mg partitioning between $(Mg,Fe)SiO_3$ post-perovskite, perovskite, and magnesiowüstite in the Earth's lower mantle. Geophys. Res. Lett. 32, L19301.

Labrosse, S., Hernlund, J.W., Coltice, N., 2007. A crystallizing dense magma ocean at the base of the Earth's mantle. Nature 450 (7171), 866–869.

Larson, A.C., Von Dreele, R.B., 2000. General Structure Analysis System (GSAS). Los Alamos National Laboratory Report LAUR, pp. 86–748.

Lay, T., Williams, Q., Garnero, E.J., 1998. The core–mantle boundary layer and deep Earth dynamics. Nature 392 (6675), 461–468.

Lee, C.A., Luffi, P., Hoink, T., Li, J., Dasgupta, R., Hernlund, J., 2010. Upside-down differentiation and generation of a 'primordial' lower mantle. Nature 463 (7283), 930–933.

Lin, J.-F., Watson, H., Vanko, G., Alp, E.E., Prakapenka, V.B., Dera, P., Struzhkin, V.V., Kubo, A., Zhao, J., McCammon, C., Evans, W.J., 2008. Intermediate-spin ferrous iron in lowermost mantle post-perovskite and perovskite. Nat. Geosci. 1 (10), 688–691.

Liu, L., 1976. The high-pressure phases of $FeSiO_3$ with implications for Fe_2SiO_4 and FeO. Earth Planet. Sci. Lett. 33 (November (1)), 101–106.

Lundin, S., Catalli, K., Santillan, J., Shim, S.-H., Prakapenka, V.B., Kunz, M., Meng, Y., 2008. Effect of Fe on the equation of state of mantle silicate perovskite over 1 Mbar. Phys. Earth Planet. Inter. 168, 97–102.

Mao, H.-K., Hemley, R.J., Fei, Y., Shu, J.F., Chen, L.C., Jephcoat, A.P., Wu, Y., Bassett, W.A., 1991. Effect of pressure, temperature, and composition on lattice parameters and density of $(Fe,Mg)SiO_3$-perovskites to 30 GPa. J. Geophys. Res. 96 (B5), 8069–8079.

Mao, H.-k., Shen, G., Hemley, R.J., 1997. Multivariable dependence of Fe–Mg partitioning in the lower mantle. Science 278 (5346), 2098–2100.

Mao, W.L., Mao, H.-k., Sturhahn, W., Zhao, J., Prakapenka, V.B., Meng, Y., Shu, J., Fei, Y., Hemley, R.J., 2006. Iron-rich post-perovskite and the origin of ultralow-velocity zones. Science 312 (5773), 564–565.

Mao, W.L., Meng, Y., Shen, G., Prakapenka, V.B., Campbell, A.J., Heinz, D.L., Shu, J., Caracas, R., Cohen, R.E., Fei, Y., 2005. Iron-rich silicates in the Earth's D″ layer. Proc. Natl. Acad. Sci. 102 (28), 9751–9753.

Mao, W.L., Shen, G., Prakapenka, V.B., Meng, Y., Campbell, A.J., Heinz, D.L., Shu, J., Hemley, R.J., Mao, H.-k., 2004. Ferromagnesian postperovskite silicates in the D″ layer of the earth. Proc. Natl. Acad. Sci. U.S.A. 101 (45), 15867–15869.

Mao, Z., Lin, J., Scott, H., Watson, H., Prakapenka, V., Xiao, Y., Chow, P., McCammon, C., 2011. Iron-rich perovskite in the Earth's lower mantle. Earth Planet. Sci. Lett. 309, 179–184.

McCammon, C., Kantor, I., Narygina, O., Rouquette, J., Ponkratz, U., Sergueev, I., Mezouar, M., Prakapenka, V., Dubrovinsky, L., 2008. Stable intermediate-spin ferrous iron in lower-mantle perovskite. Nat. Geosci. 1 (10), 684–687.

McCammon, C.A., Dubrovinsky, L., Narygina, O., Kantor, I., Wu, X., Glazyrin, K., Sergueev, I., Chumakov, A., 2010. Low-spin Fe^{2+} in silicate perovskite and a possible layer at the base of the lower mantle. Phys. Earth Planet. Inter. 180 (3–4), 215–221.

McNamara, A.K., Zhong, S., 2005. Thermochemical structures beneath Africa and the Pacific Ocean. Nature 437 (7062), 1136–1139.

Ming, L., Bassett, W., 1975. Decomposition of $FeSiO_3$ into $FeO + SiO_2$ under very high pressure and high temperature. Earth Planet. Sci. Lett. 25 (1), 68–70.

Murakami, M., Hirose, K., Kawamura, K., Sata, N., Ohishi, Y., 2004. Post-perovskite phase transition in $MgSiO_3$. Science 304 (5672), 855–858.

Oganov, A.R., Ono, S., 2004. Theoretical and experimental evidence for a post-perovskite phase of $MgSiO_3$ in Earth's D″ layer. Nature 430 (6998), 445–448.

O'Keeffe, M., Hyde, B.G., Bovin, J., 1979. Contribution to the crystal chemistry of orthorhombic perovskites: $MgSiO_3$ and $NaMgF_3$. Phys. Chem. Miner. 4 (4), 299–305.

Ono, S., Oganov, A.R., 2005. In situ observations of phase transition between perovskite and $CaIrO_3$-type phase in $MgSiO_3$ and pyrolitic mantle composition. Earth Planet. Sci. Lett. 236 (3–4), 914–932.

Rivers, M., Prakapenka, V., Kubo, A., Pullins, C., Holl, C.M., Jacobsen, S.D., 2008. The COMPRES/GSECARS gas-loading system for diamond anvil cells at the advanced photon source. High Pressure Res. 28 (3), 273–292.

Ross, N., Hazen, R., 1990. High-pressure crystal chemistry of $MgSiO_3$ perovskite. Phys. Chem Miner. 17 (3), 228–237.

Shen, G., Rivers, M.L., Wang, Y., Sutton, S.R., 2001. Laser heated diamond cell system at the Advanced Photon Source for in situ x-ray measurements at high pressure and temperature. Rev. Sci. Instrum. 72 (2), 1273.

Shieh, S.R., Duffy, T.S., Kubo, A., Shen, G., Prakapenka, V.B., Sata, N., Hirose, K., Ohishi, Y., 2006. Equation of state of the postperovskite phase synthesized from a natural $(Mg,Fe)SiO_3$ orthopyroxene. Proc. Natl. Acad. Sci. U.S.A. 103 (9), 3039–3043.

Shim, S.-H., 2008. The postperovskite transition. Ann. Rev. Earth Planet. Sci. 36 (1), 569–599.

Shim, S.-H., Duffy, T.S., Jeanloz, R., Shen, G., 2004. Stability and crystal structure of $MgSiO_3$ perovskite to the core–mantle boundary. Geophys. Res. Lett. 31, 1029–1039.

Sinmyo, R., Hirose, K., 2010. The Soret diffusion in laser-heated diamond-anvil cell. Phys. Earth Planet. Inter. 180 (3–4), 172–178.

Sinmyo, R., Hirose, K., Muto, S., Ohishi, Y., Yasuhara, A., 2011. The valence state and partitioning of iron in the Earth's lowermost mantle. J. Geophys. Res. 116, B07205.

Stackhouse, S., Brodholt, J.P., Price, G.D., 2006. Elastic anisotropy of $FeSiO_3$ end-members of the perovskite and post-perovskite phases. Geophys. Res. Lett. 33, L01304.

Stixrude, L., Lithgow-Bertelloni, C., 2011. Thermodynamics of mantle minerals—II. Phase equilbria. Geophys. J. Int. 184, 1180–1213.

Subramaniam, A.P., 1962. Pyroxenes and garnets from charnockites and associated granulites. In: Engel, A.E.J., James, H.L., Leonard, B.F. (Eds.), Petrologic Studies: A Volume in Honor of AF Buddington. Geological Society of America, New York, pp. 21–36.

Takemura, K., Dewaele, A., 2008. Isothermal equation of state for gold with a He-pressure medium. Phys. Rev. B (Condens. Matter Mater. Phys.) 78 (10), 104113–104119.

Tange, Y., Takahashi, E., Nishihara, Y., Funakoshi, K., Sata, N., 2009. Phase relations in the system MgO–FeO–SiO_2 to 50 GPa and 2000 °C: an application of experimental techniques using multianvil apparatus with sintered diamond anvils. J. Geophys. Res. 114, B02214.

Tateno, S., Hirose, K., Sata, N., Ohishi, Y., 2007. Solubility of FeO in $(Mg,Fe)SiO_3$ perovskite and the post-perovskite phase transition. Phys. Earth Planet. Inter. 160, 319–325.

Toby, B.H., 2001. EXPGUI, a graphical user interface for GSAS. J. Appl. Crystallogr. 34 (2), 210–213.

Trampert, J., Deschamps, F., Resovsky, J., Yuen, D., 2004. Probabilistic tomography maps chemical heterogeneities throughout the lower mantle. Science 306 (5697), 853–856.

Tsuchiya, T., 2003. First-principles prediction of the P-V-T equation of state of gold and the 660-km discontinuity in Earth's mantle. J. Geophys. Res. 108, 2462.
Williams, Q., Garnero, E.J., 1996. Seismic evidence for partial melt at the base of Earth's mantle. Science 273 (5281), 1528–1530.
Wysession, M.E., Lay, T., Revenaugh, J., Williams, Q., Garnero, E.J., Jeanloz, R., Kellogg, L.H., 1998. The D″ discontinuity and its implications. In: Gurnis, M., Wysession, M.E., Knittle, E., Buffett, B.A. (Eds.), The Core–mantle Boundary Region. Geodynamics Series, vol. 28. American Geophysical Union, pp. 273–297.
Yagi, T., Mao, H.-K., Bell, P., 1979. Lattice parameters and specific volume for the perovskite phase of ortho-pyroxene composition, (Mg,Fe)SiO_3. Carnegie Inst. Washington Year Book 78 (1790), 612–613.
Yamanaka, T., Mao, W.L., Mao, H.-k., Hemley, R.J., Shen, G., 2010. New structure and spin state of iron-rich (Mg,Fe)SiO_3 post-perovskite. J. Phys.: Conf. Ser. 215, 012100.
Zhang, L., Meng, Y., Mao, W.L., 2012. Effect of pressure and composition on lattice parameters and unit-cell volume of (Fe,Mg)SiO_3 perovskite. Earth Planet. Sci. Lett., 317–318 120–125.